



ANGPTL4 binds to the leptin receptor to regulate ectopic bone formation

Hongling Hu^{a,b,1}, Sheng Luo^{c,1} , Pinglin Lai^{a,1}, Mingqiang Lai^{d,1}, Linlin Mao^e, Sheng Zhang^e, Yuanjun Jiang^e, Jiaxin Wen^e, Wu Zhou^e, Xiaolin Liu^e, Liang Wang^a, Minjun Huang^a , Yanjun Hu^f, Xiaoyang Zhao^g , Laixin Xia^g, Weijie Zhou^h , Yu Jiangⁱ, Zhipeng Zou^e , Anling Liu^{c,2}, Bin Guo^{e,j,2}, and Xiaochun Bai^{a,e,2}

Edited by Gérard Karsenty, Columbia University, New York, NY; received June 25, 2023; accepted November 17, 2023 by Editorial Board Member David J. Mangelsdorf

Leptin protein was thought to be unique to leptin receptor (LepR), but the phenotypes of mice with mutation in LepR [*db/db* (diabetes)] and leptin [*ob/ob* (obese)] are not identical, and the cause remains unclear. Here, we show that *db/db*, but not *ob/ob*, mice had defect in tenotomy-induced heterotopic ossification (HO), implicating alternative ligand(s) for LepR might be involved. Ligand screening revealed that ANGPTL4 (angiopoietin-like protein 4), a stress and fasting-induced factor, was elicited from brown adipose tissue after tenotomy, bound to LepR on PRRX1⁺ mesenchymal cells at the HO site, thus promotes chondrogenesis and HO development. Disruption of LepR in PRRX1⁺ cells, or lineage ablation of LepR⁺ cells, or deletion of ANGPTL4 impeded chondrogenesis and HO in mice. Together, these findings identify ANGPTL4 as a ligand for LepR to regulate the formation of acquired HO.

leptin receptor | ANGPTL4 | heterotopic ossification

Ob/ob and *db/db* mice are two of the most intensively studied genetic mutant mouse models. Since the discovery of the mouse leptin protein [encoded by the obese (*ob*) gene] and the identification of the leptin receptor (LepR) [encoded by the diabetes (*db*) gene], numerous studies have described the critical roles of leptin-LepR in regulating central aspects of energy homeostasis, glucose uptake, and appetite (1–5). *Ob/ob* and *db/db* mice share many phenotypes, and for decades, the mouse leptin protein was thought to be unique to LepR (6). However, their phenotypes are not identical, and the cause remains ambiguous (7).

Leptin is produced by adipocytes and regulates bone metabolism partly by acting through LepR on hypothalamic neurons to activate the sympathetic nervous system, which inhibits osteoblast proliferation (8–10). LepR is also expressed in skeletal cells, such as mesenchymal stem cells (MSCs), the major source of osteoblasts and adipocytes in bone marrow (11, 12). However, the direct role of leptin-LepR in regulating bone metabolism has been debated due to conflicting results. For example, leptin has been shown to promote osteogenesis of cultured MSCs in some studies (13) but inhibit osteogenesis in other studies (14). It has also been reported to inhibit adipogenesis in cultured MSCs (13), but deletion of LepR in MSCs using *Prrx1-Cre* promoted osteogenesis while inhibiting adipogenesis in mice (15). Besides, *ob/ob* and *db/db* mice were shown to have significant difference in bone metabolic phenotype (16). The above evidence implicates that leptin may not be the only ligand for LepR. Thus, the undiscovered alternative ligands for LepR and their efficacy in controlling physiological homeostasis may be of therapeutic value.

Acquired heterotopic ossification (HO), an aberrant but tightly orchestrated regenerative process with ectopic bone formation, occurs within normally unmineralized tissues in response to trauma, surgery, or burns (17–19). It is an endochondral ossification process, including initial chondrogenesis, followed by chondrocyte hypertrophy and heterotopic mineralization, and finally the formation of mature bone with bone marrow (20, 21). Although the cell precursors of HO are complicated, and much has been learned from transgenic reporter animals to identify the cell types putatively responsible for the formation of HO (20, 22–25), the aggregate data suggest that the predominant source of HO is generally from stromal cells of mesenchymal origin, which can be labeled using *Prrx1-Cre* (17). However, how the injuries stimulate chondrogenesis of mesenchymal cells is unclear, and the role for LepR in this process has not been reported.

The present study found that *db/db* but not *ob/ob* mice had severe defect in HO development. We show that in response to tenotomy, angiopoietin-like protein 4 (ANGPTL4), a stress and fasting-induced secreting protein (26–29), is elicited from the brown adipose tissue (BAT) and promotes the chondrogenic process by directly binding to LepR on

Significance

Leptin-deficient *ob/ob* (obese) mice and leptin receptor (LepR)-deficient *db/db* (diabetes) mice are commonly used models mimicking conditions of obesity and type 2 diabetes. However, their phenotypes are not identical, and the cause remains ambiguous. Here, we found that *db/db*, but not *ob/ob*, have defect in the development of acquired heterotopic ossification (HO), an aberrant bone formation process in response to trauma, surgery, or burns. Thus, we screened for alternative LepR-binding proteins and found that ANGPTL4 (angiopoietin-like protein 4) bound to LepR on mesenchymal cells at the HO site to promote HO development. Indeed, the present work adds to the known regulatory mechanisms of HO development to propagate a paradigm shift in the approach to manage the pathogenesis of acquired HO.

Author contributions: H.H., X.Z., L.X., W.Z., Y.J., Z.Z., A.L., B.G., and X.B. designed research; H.H., S.L., P.L., M.L., L.M., S.Z., Y.J., J.W., W.Z., X.L., L.W., M.H., and Y.H. performed research; H.H., S.L., P.L., M.L., M.H., Y.H., and X.B. analyzed data; and B.G. and X.B. wrote the paper.

The authors declare no competing interest.

This article is a PNAS Direct Submission. G.K. is a guest editor invited by the Editorial Board.

Copyright © 2023 The Author(s). Published by PNAS. This article is distributed under Creative Commons Attribution-NonCommercial-NoDerivatives License 4.0 (CC BY-NC-ND).

¹H.H., S.L., P.L., and M.L. contributed equally to this work.

²To whom correspondence may be addressed. Email: aliu@smu.edu.cn, bzg18@smu.edu.cn, or baixc15@smu.edu.cn.

This article contains supporting information online at <https://www.pnas.org/lookup/suppl/doi:10.1073/pnas.2310685120/-DCSupplemental>.

Published December 26, 2023.

PRRX1⁺ mesenchymal cells at the HO site. Together, these data establish ANGPTL4 as a ligand for LepR in regulating ectopic bone formation, suggest that LepR⁺ cells may modulate bone metabolism under physiological and pathological conditions by binding alternative ligands other than leptin, and implicate that targeting ANGPTL4–LepR has therapeutic potential for acquired HO disorders.

Results

LepR But Not Leptin Is Essential for the Development of Acquired HO. HO is a tightly orchestrated bone formation event which occurs within normally unmineralized tissues, for example, the Achilles tendon. In tenotomy-induced acquired HO mouse model (*SI Appendix*, Fig. S1), the ectopic bone formation process is characterized by acute inflammation stage (0 to 2 wk), initial chondrogenesis stage (2 to 4 wk), and osteogenesis stage (4 to 8 wk).

To investigate the potential role of leptin–LepR signaling in ectopic bone formation, incisions were made on the Achilles's tendon of *db/db* and *ob/ob* mice, and HO process was monitored at 3 wk, 8 wk, and 16 wk after the surgery via micro computed tomography (Micro-CT) analysis and a series of staining (Fig. 1 and *SI Appendix*, Fig. S2). Comparing *ob/ob* mice to age- and sex-matched wild-type negative controls (termed NC) at 3 wk, a representative time point for evaluating chondrogenesis process, no significant difference was observed as indicated by hematoxylin and eosin (H&E) staining (Fig. 1B), safranin O and fast green (SOGF) staining (Fig. 1C), immunofluorescence staining for Aggrecan (Fig. 1D) and masson staining (Fig. 1E). However, in *db/db* mice that underwent tenotomy, no cartilage tissue was observed at 3 wk (Fig. 1 B–E). Most interestingly, at 8 wk, where Micro-CT images and Immunohistochemistry (IHC) analysis for OCN revealed that *ob/ob* mice and NC mice developed ectopic bone at the injured site, *db/db* mice failed in the formation of acquired HO (Fig. 1 A, F, and H). And when evaluated 16 wk after tenotomy, *db/db* mice only developed a negligible amount of acquired HO (Fig. 1H and *SI Appendix*, Fig. S2). Consistent with this, using *LepR-Cre* inducible diphtheria toxin receptor (*iDTR*) transgenic mice (*LepR-Cre;iDTR*) (Fig. 2A), DT-induced lineage ablation of LepR⁺ cells prevented the tenotomy-induced HO formation at 8 wk after the surgery (Fig. 2 B and C). Together, these findings suggest that LepR, but not leptin, is necessary for the chondrogenic process in the development of acquired HO, implying that alternative ligand(s) other than leptin bind(s) to and regulate(s) LepR actions on ectopic bone formation.

Chondrogenesis during Acquired HO Formation Requires LepR on PRRX1⁺ Mesenchymal Cells. To gain mechanistic insight into the observed impediment to acquired HO formation in *db/db* mice and DT-treated *LepR-Cre;iDTR* mice, we monitored the involvement of LepR⁺ cells throughout the HO development process by generating *LepR-Cre;mTnG* mice. Fluorescence images revealed the localization of large amounts of LepR⁺ cells at the HO site during initial chondrogenic process (HO 3 wk) (Fig. 2D), where PRRX1⁺ mesenchymal cells differentiate into chondrocytes (22), and retained population during osteogenesis stage (HO 8 wk) (Fig. 2E). In light of previous studies revealing that mesenchymal cells play a critical role during chondrogenesis and osteogenesis (22), and over 90% of PRRX1⁺ mesenchymal cells express LepR (11), we generated *Prx1-Cre;LepR^{fl/fl}* mice (Fig. 3A) to further dissect the role of LepR in the pathology of acquired HO. To verify knock-out efficiency, western blotting analysis (Fig. 3B) and immunofluorescence experiments (Fig. 3C) with primary BMSCs were performed. Both analyses presented significant reduction in LepR mRNA or protein level (Fig. 3 B and C). Next, a comparison of the ability to develop acquired HO

was conducted between the *Prx1-Cre;LepR^{fl/fl}* knockout mice and the control littermates. Measurements of HO volume (Fig. 3E) based on Micro-CT images (Fig. 3D) and H&E staining results (Fig. 3F), SOGF (Fig. 3G), and Aggrecan (Fig. 3H) confirmed that loss of LepR on PRRX1⁺ mesenchymal cells restrained the chondrogenesis process during acquired HO formation (Fig. 3 D–J). In addition, to examine the involvement of LepR on chondrocytes and osteocytes during the second half of HO formation (chondrocyte hypertrophy and heterotopic mineralization, and finally the formation of mature bone with bone marrow), *Col2a1-Cre;LepR^{fl/fl}* mice and *Dmp1-Cre;LepR^{fl/fl}* mice were generated, respectively. Micro-CT results revealed that the mice's ability to develop acquired HO was not compromised by the loss of LepR on chondrocytes or osteocytes (*SI Appendix*, Fig. S3 G and H). Together, these data indicate that LepR on mesenchymal cells play critical role during initial chondrogenic process (HO 3 wk) of HO formation.

ANGPTL4 Binds to LepR at Higher Affinity than Leptin. The above-observed difference between *db/db* and *ob/ob* mice in HO development provides a rationale to search for additional LepR-binding proteins affecting the pathogenesis of acquired HO. Thus, we collected serum from the HO group (4 wk after tenotomy) and sham controls. The time point was chosen because HO can be easily observed at 4 wk but not 3 wk to confirm the success of tenotomy. Surface plasmon resonance (SPR), high-performance liquid chromatography, and matrix-assisted laser desorption ionization time-of-flight mass spectrometry techniques were then performed with collected serum samples to capture and test the target proteins of LepR. A total of 20 secreted proteins in serum interacting with LepR were identified by mass spectrometry, including a set of 2 proteins that were only detected in HO group (*SI Appendix*, Table S1 and Fig. 4A). Among these potential targets, ANGPTL4, whose difference in enrichment between HO and NC groups was the largest, was chosen for further study (Fig. 4A and *SI Appendix*, Table S1). ANGPTL4 is a stress and fasting-induced secreted protein highly expressed in metabolic tissues, prominently in adipose tissue and liver (30). It has been shown to act as a serum hormone that regulates lipid metabolism by inhibiting lipoprotein lipase activity (31). We further performed SPR binding-affinity measurement of both leptin and ANGPTL4 with LepR and found that leptin or ANGPTL4 bound to LepR in dose-dependent manners (Fig. 4 D and E). Surprisingly, SPR demonstrated that ANGPTL4 bound to LepR at higher affinity (ABS (tr_KD) = 21.924) than leptin (ABS (tr_KD) = 8.103) (Fig. 4 B and C and *SI Appendix*, Table S2), reframing our understanding of leptin–LepR signaling axis.

Regions of the LepR protein and ANGPTL4 protein responsible for interaction were next studied. The 3D structure of proteins LepR (Fig. 4F) and ANGPTL4 (Fig. 4G) were downloaded from AlphaFold Protein Structure Database (<https://alphafold.ebi.ac.uk/>) and the ID of LepR and ANGPTL4 are AF-P48356-F1-model_v2 and AF-Q9Z1P8-F1-model_v2, respectively. Computational molecular docking modeling indicated that Tyr26, Ile169, Asp170, Asp171, Lys178, Asn205, Gln229, and Arg310 the residues in LepR were involved in binding with Arg187, Arg190, Gln193, Gln197, Asp225, Gly271, Arg273, Gln276, Gln292, Asn324, Gln402, and Ser410 in ANGPTL4 through salt bridges and hydrogen bond interactions (Fig. 4 H and I). The above suggested that the N-terminal of LepR and the C-terminal of ANGPTL4 might be the interacting sites. Next, we generated FLAG-tagged full-length LepR (FLAG-LepR), FLAG-tagged NT (amino acids) aa22 to aa496 of LepR (FLAG-LepR-N), FLAG-tagged CT aa497 to aa839 of LepR (FLAG-LepR-C), and GST-tagged full-length ANGPTL4 (GST-ANGPTL4) constructs (Fig. 4J). GST-tagged

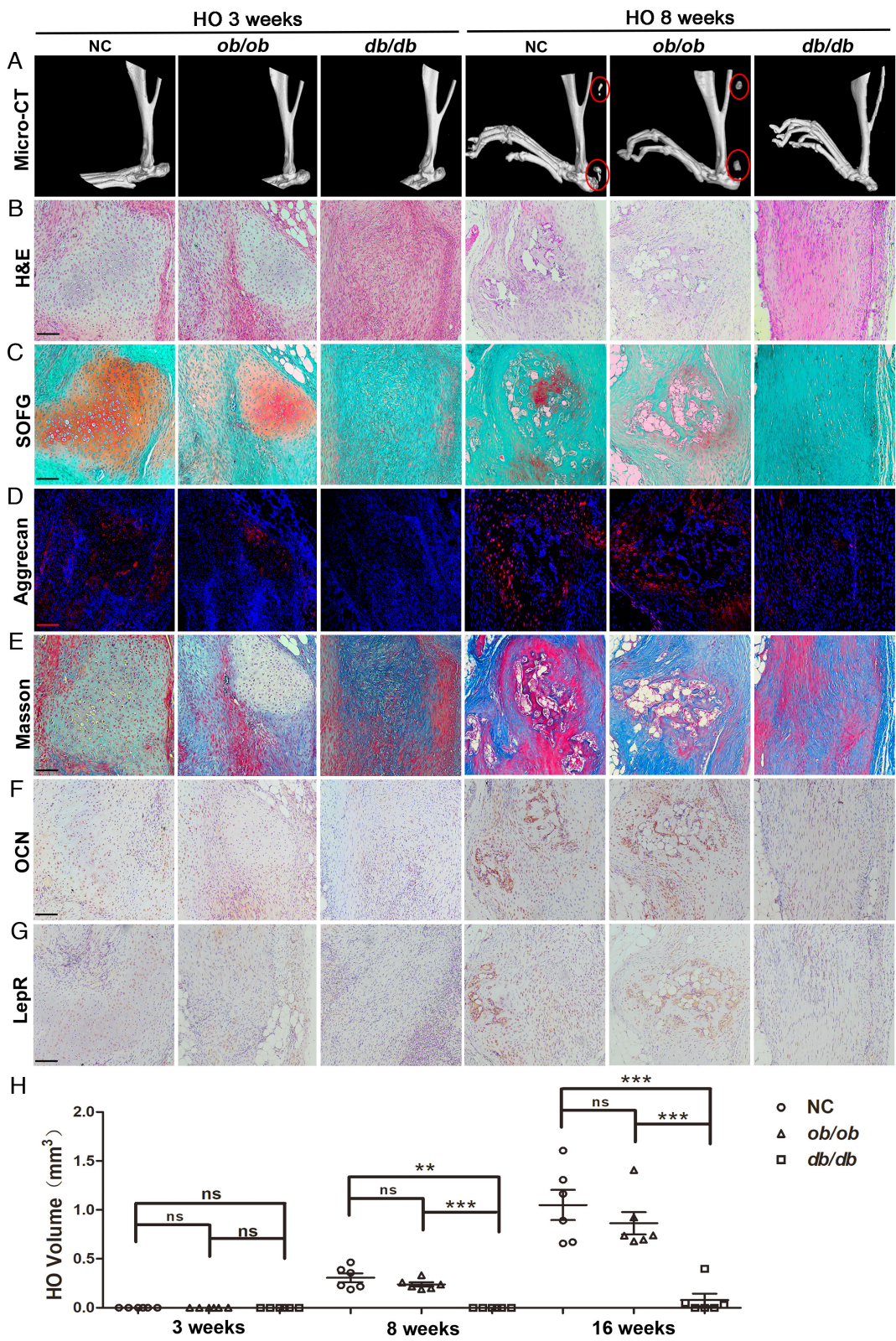


Fig. 1. *db/db* but not *ob/ob* mice exhibit defect in the formation of acquired HO. (A) Representative Micro-CT three-dimensional (3D) modeling images of Achilles tendon (sagittal view) of mice in indicated group 3 wk (early chondrogenesis stage, *Left*) or 8 wk (early osteogenesis stage, *Right*) after tenotomy. Red ovals indicate ectopic bones. (B–G) Representative images for (B) H&E staining, (C) SOFG staining [proteoglycan (red), heterotopic bone and Achilles tendon (green)], (D) IF staining for Aggrecan (red) and DAPI (blue), (E) Masson staining, (F) IHC staining for OCN, and (G) IHC staining for LepR of Achilles tendon of mice in indicated group 3 wk or 8 wk after tenotomy. (Scale bars, 100 μ m.) (H) Quantification of Fig. 1A and *SI Appendix*, Fig. S2 showing HO volumes of mice in indicated group ($n = 6$ to 8 mice per group). Data are represented as mean \pm SEM. ns, no significance; * P < 0.05, ** P < 0.01, *** P < 0.001. See also *SI Appendix*, Figs. S1 and S2.

full-length Leptin (GST-Leptin) served as positive control. Co-immunoprecipitation (co-IP) analysis revealed that full-length LepR and fragment containing the N-terminal of LepR can pull

down ANGPTL4 (Fig. 4K and Fig. 4L, *Upper*), fragment without the N-terminal loses its ability to interact with ANGPTL4 (Fig. 4L, *Lower*). Meanwhile, knockout of the N-terminal proportion of

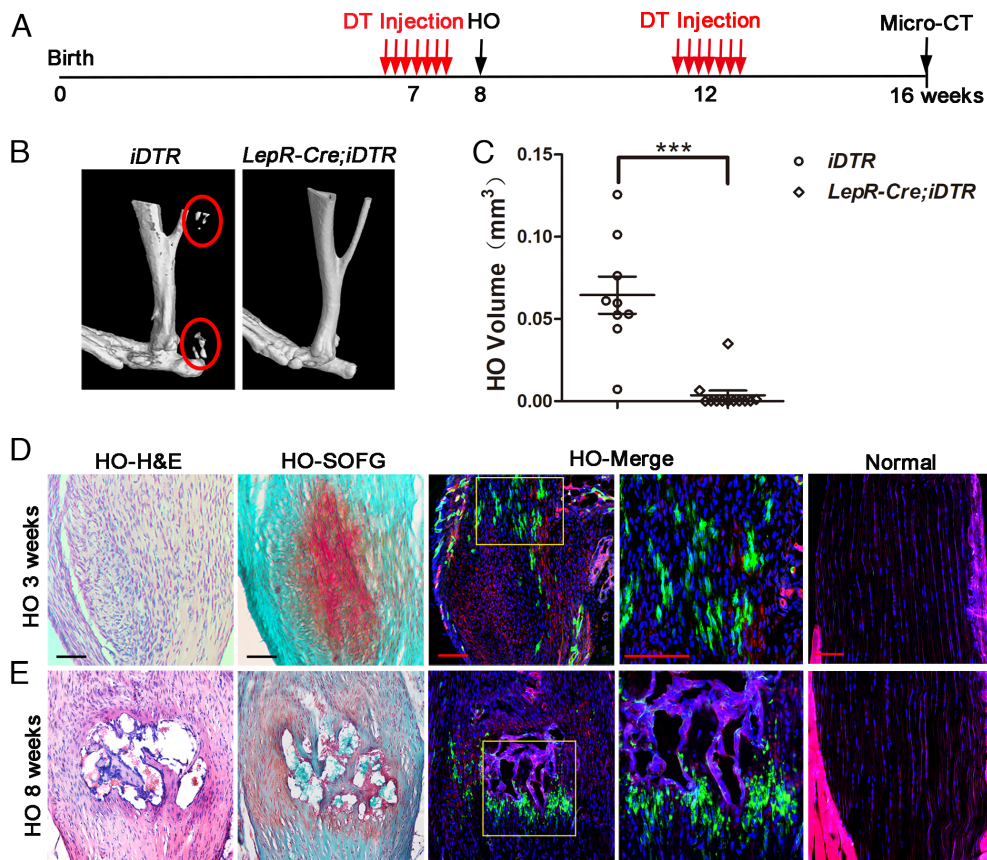


Fig. 2. LepR⁺ cells contribute to the formation of acquired HO. (A) Schematic of experimental strategy. (B) Representative Micro-CT 3D modeling images of Achilles tendon (sagittal view) of mice in indicated group 8 wk after tenotomy. Red ovals indicate ectopic bones. (C) Quantification of B showing HO volumes of mice in indicated group ($n = 9$ to 12 mice per strain). Data are represented as mean \pm SEM. *** $P < 0.001$. (D and E) Representative images for H&E staining, SOFG staining [proteoglycan (red); heterotopic bone and Achilles tendon (green)], and IF staining for DAPI (blue; LepR⁺ cells express membrane-bound GFP instead of tomato fluorescent protein) of Achilles tendon of mice in indicated group (D) 3 wk or (E) 8 wk after tenotomy. (Scale bars, 100 μ m.)

ANGPTL4 did not affect the development of acquired HO (Fig. 4 M and N), suggesting ANGPTL4's regulation of ectopic bone formation could be C-terminal related. In addition, immunofluorescence staining with samples from the HO site revealed elevated protein level of ANGPTL4 (green) and its co-localization with LepR (red) (Fig. 4 O), further supporting the binding between ANGPTL4 and LepR.

iBAT (interscapular BAT) Produces and Secretes ANGPTL4 after Tenotomy. To explore the origin of ANGPTL4, we performed *in situ* expression studies in the surrounding bone and soft tissues areas developing ectopic bone formation post-surgery. Immunofluorescence staining with samples from the surgery/HO site revealed negligible protein levels of ANGPTL4 (red) in the bone-related area (labeled as "B") and surrounding skeletal muscle (labeled as "M") both with and without the surgery (3 wk post tenotomy) (Fig. 5 A). To further confirm that the surrounding skeletal muscle does not secrete ANGPTL4 to regulate HO formation, we surgically ablated the gastrocnemius muscle, the soleus muscle, and the plantaris muscle of the mice during the tenotomy surgery. Micro-CT images showed that muscle ablation did not affect the formation of HO (Fig. 5 B), further eliminating the involvement of the surrounding skeletal muscle. In addition, we collected heart, liver, white adipose tissue (WAT), iBAT, and skeletal muscle and attached tendon (labeled as "M + T") from wild-type C57BL/6 mice which underwent the tenotomy surgery and sham controls. While liver, WAT, and iBAT had decent mRNA levels of *Angptl4*, elevations in *Angptl4* levels along with the formation of HO were only observed in iBAT (Fig. 5 C). And the elevations in iBAT

Angptl4 mRNA levels corresponded with the elevations in serum ANGPTL4 concentrations (Fig. 5 D). Last but not least, we surgically ablated iBAT to confirm its critical role in secreting ANGPTL4 and in regulating HO formation. Measurements of serum ANGPTL4 concentration revealed that at 3 wk post tenotomy, where a significant elevation was observed in wild-type C57BL/6 mice that underwent the surgery, iBAT-ablated mice had only a slight but not significant increase in serum ANGPTL4 concentration comparing to negative control group (NC) (Fig. 5 D). Consistent with this, measurements of HO volume (Fig. 5 G) based on Micro-CT images (Fig. 5 F) and SOFG staining results (Fig. 5 E) confirmed that loss of iBAT restrained the acquired HO formation. Together, these findings indicate that BAT-secreted ANGPTL4 is a critical and essential regulator of tenotomy-induced ectopic bone formation.

In addition, the involvement of ANGPTL4 in chondrogenesis under normal physiological conditions was examined. Growth of the longitudinal bone occurs at the growth plate, a cartilage structure that harbors chondrocyte proliferation, hypertrophy, and cartilage matrix secretion resulting in chondrogenesis (32). During this physiological chondrogenic process, ANGPTL4 was not visualized at the growth plate (SI Appendix, Fig. S4). Together, these data indicate that ANGPTL4, which is secreted from BAT after tenotomy, directly binds to LepR in regions with tenotomy-induced ectopic bone formation.

ANGPTL4 Promotes Chondrogenesis of Mesenchymal Cells and HO Development via LepR. Since LepR on PRRX1⁺ mesenchymal cells was shown above to be essential for the development of acquired

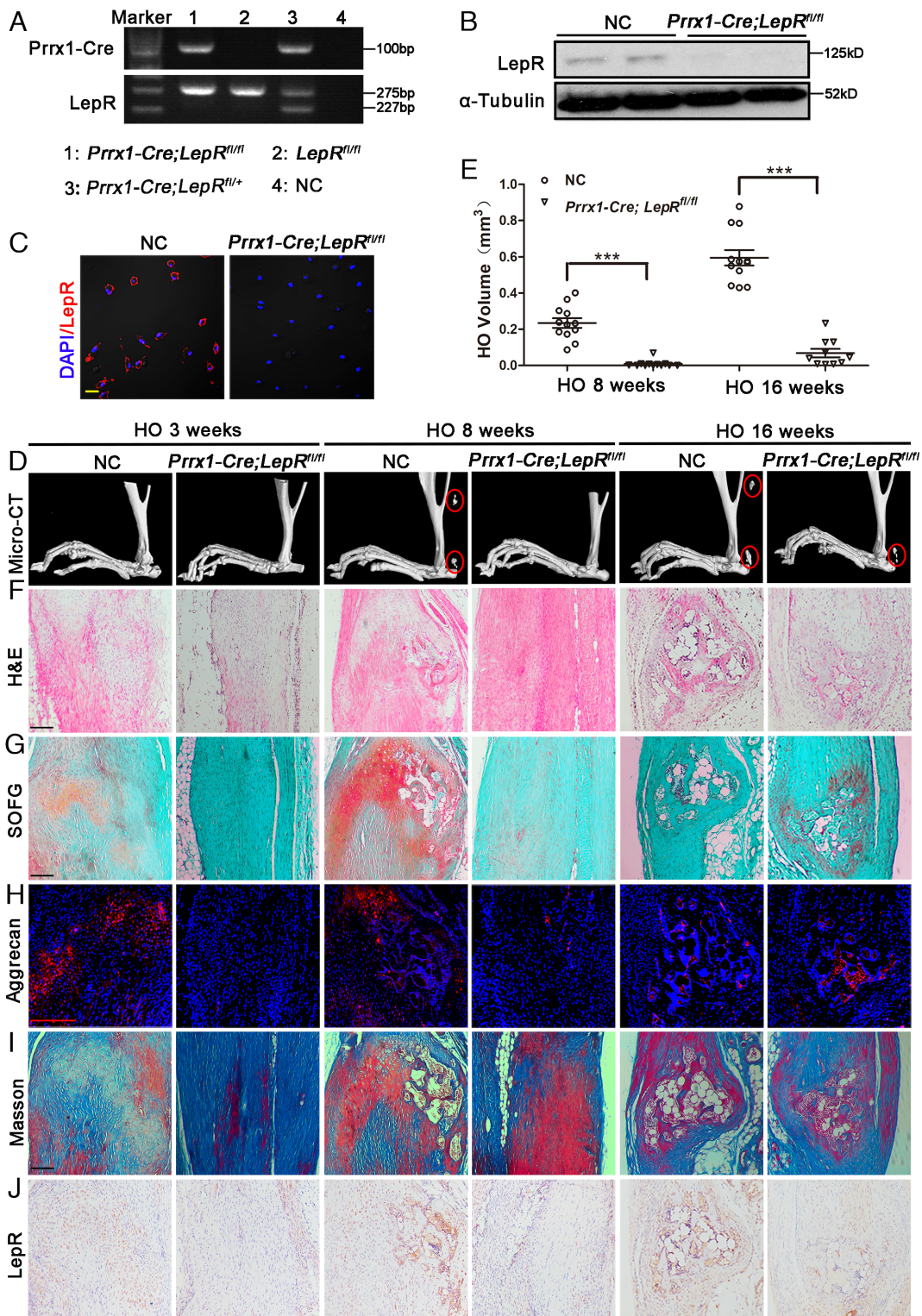


Fig. 3. LepR on PRRX1⁺ mesenchymal cells is required for the formation of acquired HO. (A) Representative genotyping results of *Prrx1-Cre;LepR^{fl/fl}* or control littermates. Primers used in this experiment are listed in Key Resources Table. (B) Western blotting analysis of LepR expression in primary BMSCs isolated from *Prrx1-Cre;LepR^{fl/fl}* or control littermates. α-Tubulin was used as loading control. (C) Representative images for IF staining for LepR (red) and DAPI (blue) in primary BMSCs isolated from *Prrx1-Cre;LepR^{fl/fl}* or control littermates. (Scale bar, 20 μm.) (D) Representative Micro-CT 3D modeling images of Achilles tendon (sagittal view) of mice in indicated group 3 wk, 8 wk, or 16 wk (late osteogenesis stage, Right) after tenotomy. Red ovals indicate ectopic bones. (E) Quantification of D showing HO volumes of mice in indicated group (n = 9 to 12 mice per group). Data are represented as mean ± SEM. ***p < 0.001. (F–J) Representative images for (F) H&E staining, (G) SOFG staining [proteoglycan (red), heterotopic bone and Achilles tendon (green)], (H) IF staining for Aggrecan (red) and DAPI (blue), (I) Masson staining, and (J) IHC staining for LepR of Achilles tendon of mice in indicated group 3 wk, 8 wk, or 16 wk after tenotomy. (Scale bars, 100 μm.) *SI Appendix, Fig. S3*.

HO, ANGPTL4 impacts on LepR-mediated regulation on HO were further explored, particularly with respect to chondrogenesis of mesenchymal cells. In vitro, exogenous ANGPTL4 (10 ng/mL) protein enhanced toluidine blue staining of human umbilical cord

MSCs (hUC-MSCs), indicating promoted chondrodifferentiation (Fig. 6A). Meanwhile, consistent with results from the affinity test (Fig. 4 B–E), equal amount of leptin protein (10 ng/mL) had a milder effect on hUC-MSCs chondrogenesis than ANGPTL4

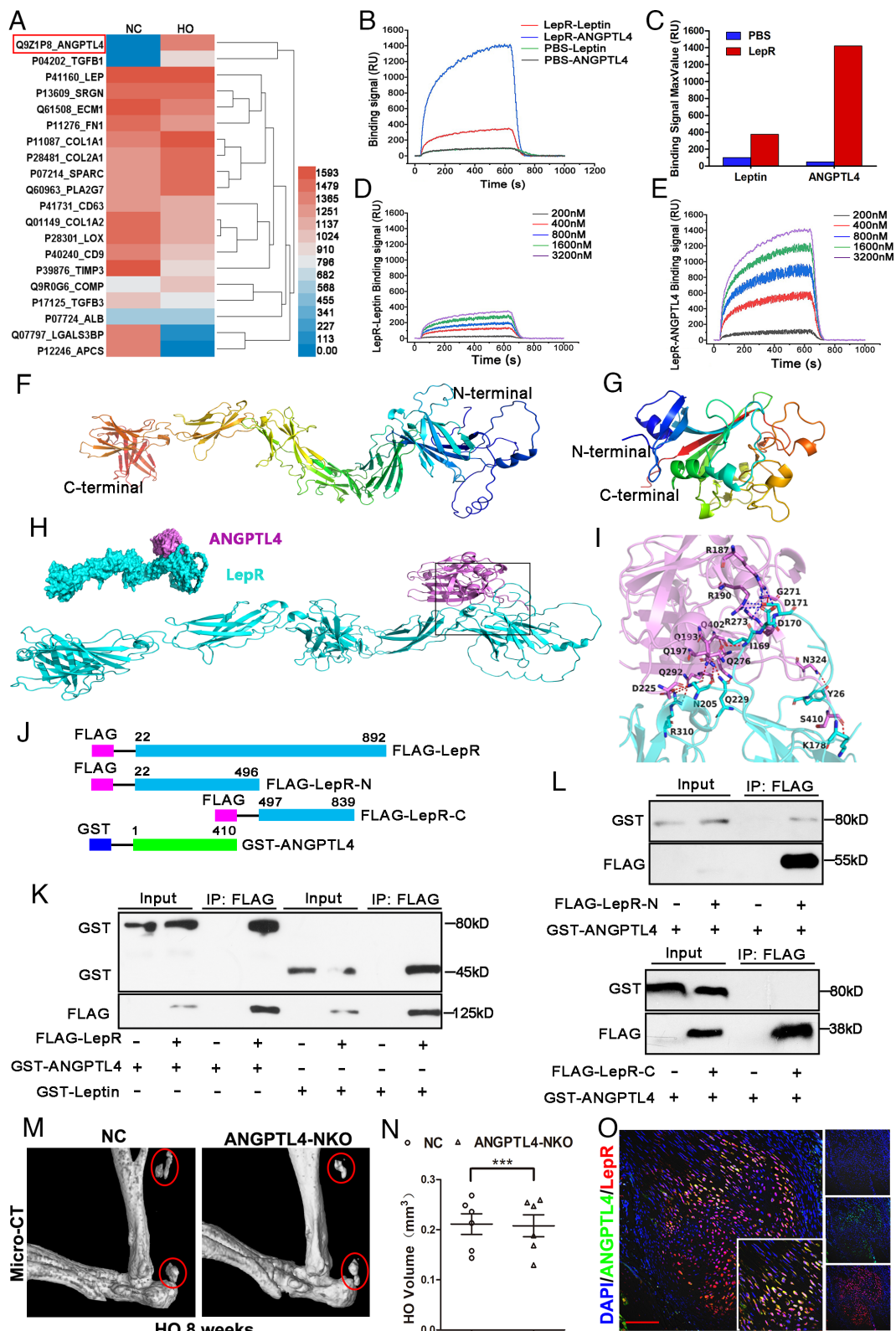


Fig. 4. ANGPTL4 binds to LepR at higher affinity than leptin. (A) Heatmap of the most highly differentially expressed LepR-interacting proteins from “HO 4 wk” or control mice serum. (B) Binding response curves of LepR-Leptin and LepR-ANGPTL4. (C) Binding affinity described in B. (D and E) SPRI assay involving (D) LepR and leptin or (E) LepR and ANGPTL4. (F–I) The predicted 3D structure of (F) LepR, (G) ANGPTL4, (H) binding model for ANGPTL4 (purple) with LepR (blue), and (I) detailed interaction model for ANGPTL4 (purple) with LepR (blue), the residues in ANGPTL4 are shown as violet sticks, the residues in LepR are shown as cyan sticks, the red dashes represent hydrogen bond interaction, the blue dashes represent salt bridge. (J) Schematic diagram of LepR and ANGPTL4 constructs: FLAG-tagged LepR amino acids (aa) 22 to 892 (FLAG-LepR), FLAG-tagged LepR N-terminal aa 22 to 496 (FLAG-LepR-N), FLAG-tagged LepR C-terminal aa 497 to 839 (FLAG-LepR-C) and GST-tagged full-length ANGPTL4 aa 1 to 410 (GST-ANGPTL4). (K) Representative results for co-IP assays of exogenous FLAG-tagged LepR with GST-tagged ANGPTL4 or GST-tagged Leptin in HEK293 cells. (L) Representative results for co-IP assays of exogenous FLAG-tagged LepR-N (Upper) or FLAG-tagged LepR-C (Lower) with GST-tagged ANGPTL4 in HEK293 cells. (M) Representative Micro-CT 3D modeling images of Achilles tendon (sagittal view) of mice in indicated group 8 wk after tenotomy. Red ovals indicate ectopic bones. (N) Quantification of L showing HO volumes of mice in indicated group ($n = 6$ mice per strain). Data are represented as mean \pm SEM. *** $P < 0.001$. (O) Representative IF staining images revealing co-localization of LepR (red) and ANGPTL4 (green) at HO site. (Scale bar, 100 μ m.)

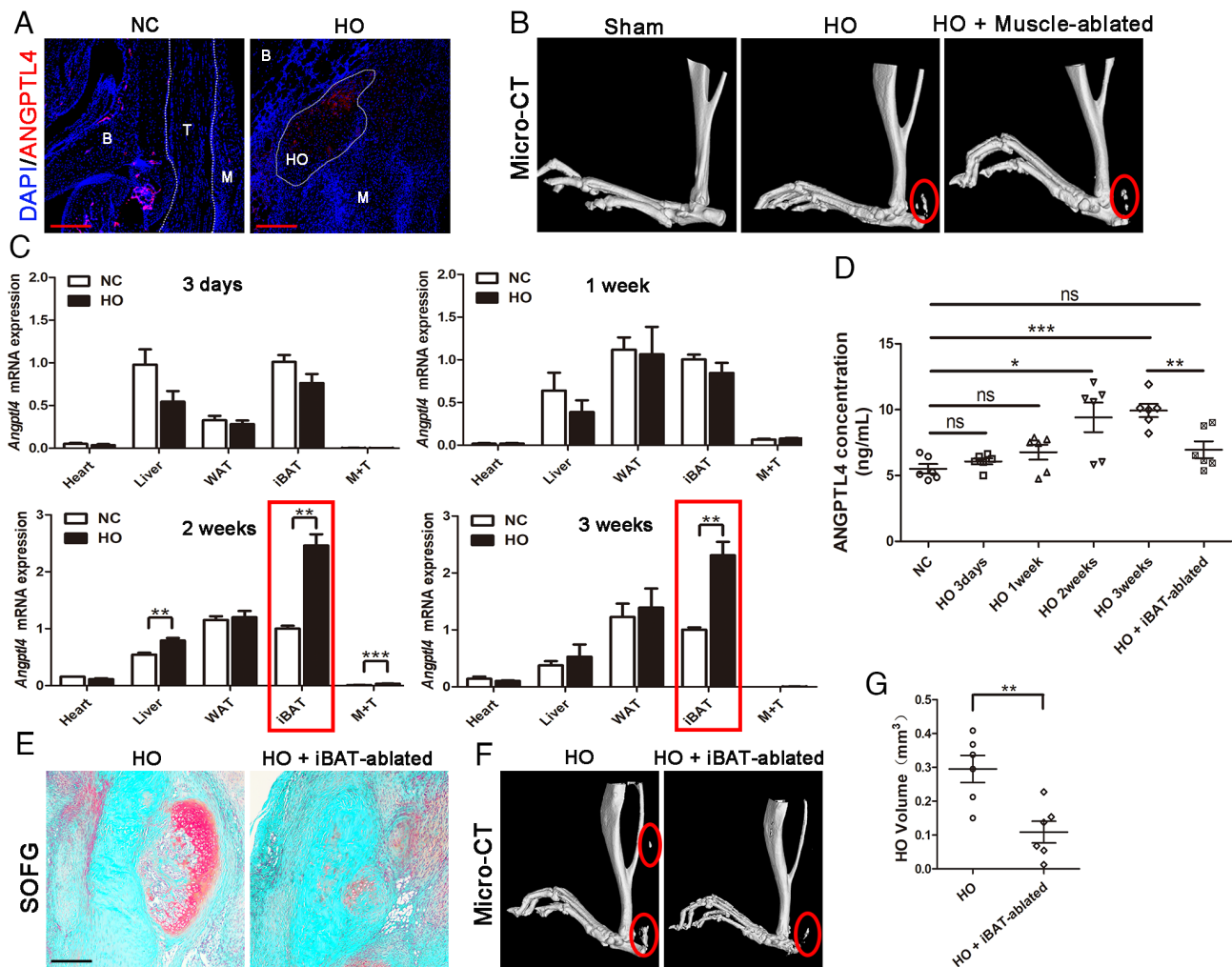


Fig. 5. iBAT produces and secretes ANGPTL4 after tenotomy. (A) Representative IF staining images of ANGPTL4 (red) at normal tendon, muscle, and tenotomy 3 wk HO site. T, tendon; M, muscle; HO, heterotopic ossification. (Scale bar, 100 μ m.) (B) Representative images for Micro-CT 3D modeling of Achilles tendon (sagittal view) of mice in indicated group 8 wk after tenotomy. Red ovals indicate ectopic bones. (C) *Angptl4* mRNA expression level in indicated tissue normalized to β -actin. The fold change was normalized to the expression in iBAT in the NC group. n = 4 mice per group. Data are represented as mean \pm SEM. WAT, white adipose tissue; iBAT, interscapular brown adipose tissue; M+T, Muscle and Tendon. ** $P < 0.01$, *** $P < 0.001$. (D) Enzyme-linked immunosorbent assay analysis of serum ANGPTL4 level in mice from indicated group. n = 6 per group. Data are represented as mean \pm SEM. ns, no significance; * $P < 0.05$, *** $P < 0.001$. (E) Representative images for SOFG staining [proteoglycan (red), heterotopic bone and Achilles tendon (green)] of Achilles tendon of mice in indicated strain 3 wk after tenotomy. (Scale bars, 100 μ m.) (F) Representative images for Micro-CT 3D modeling of Achilles tendon of mice in indicated strain 8 wk after tenotomy. (G) Quantification of F showing HO volumes of mice in indicated strain (n = 6 mice per strain). Data are represented as mean \pm SEM. ** $P < 0.01$. See also SI Appendix, Fig. S4.

(Fig. 6*A*). As expected, *in vivo* Micro-CT imaging of phosphate buffered solution (PBS)- or ANGPTL4-treated (5 ng/g of body weight through tail vein, 3 times per week for 8 wk) mice confirmed increased HO volume in ANGPTL4-treated mice 8 wk after tenotomy (Fig. 6*B* and *C*).

In addition, we generated a LepR-KO mesenchymal stem cell line (MSC) by deleting parts of exon 3 and exon 4 (SI Appendix, Fig. S5 *A* and *B*). As indicated by toluidine blue staining results, loss of LepR hindered the pro-chondrogenesis effect of ANGPTL4 (Fig. 6*D*), supporting the LepR-dependent role of ANGPTL4 in chondrogenesis of mesenchymal cells. Next, we generated a knockout mouse model for ANGPTL4 (termed “ANGPTL4-KO”) (Fig. 6*E* and SI Appendix, Fig. S5*C*). In this method, loss of ANGPTL4 blocked the chondrogenesis process and development of acquired HO (Fig. 6*G* and *H*), confirming the vital role of ANGPTL4 in ectopic bone formation.

ANGPTL4-LepR Activates STAT3 (Signal Transducer and Activator of Transcription 3) to Promote Chondrogenesis in MSCs. ANGPTL4-LepR impacts on chondrogenesis were further explored, particularly with respect to potential downstream signaling pathways.

To characterize the effects of exogenous ANGPTL4 on hUC-MSCs in terms of phosphorylation changes, starvation was performed prior to stimulation to lower basal phosphorylation levels. Phosphoproteomics analysis identified more than 1,150 proteins, of which 486 proteins were recognized as hyperphosphorylated in ANGPTL4-treated hUC-MSCs (SI Appendix, Table S3). Molecular function pathway enrichment analysis revealed that the most significant functional category is lamin binding (Fig. 7*A*), among these are two proteins, lamina-associated polypeptide 2 (TMPO) and lamin B receptor, whose phosphorylation states influence their lamin-related roles (33–35). Lamins and lamin-binding proteins have been associated with developmental progression, cell differentiation, and tissue-specific functions (36, 37). Although the specific roles for lamins in bone development and metabolism need further dissection, their potential values have been suggested by several studies (38, 39). Among all the phosphoproteins, nestin (NES), gap junction protein alpha 1, and STAT3 were most significantly hyperphosphorylated in ANGPTL4 group (Fig. 7*B*). As STAT3 signaling pathway is known to play essential roles in the differentiation of various cell types (40, 41), including

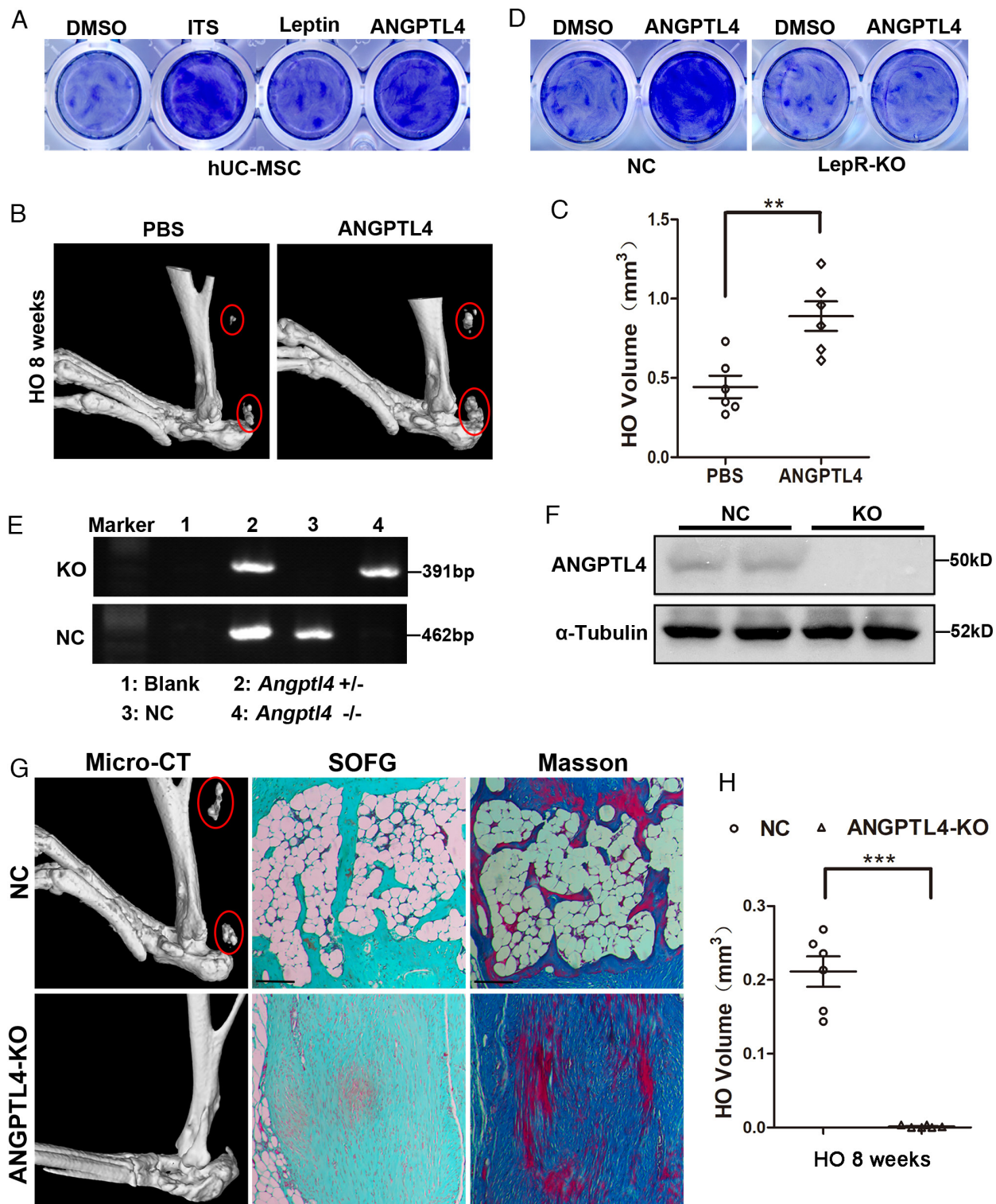


Fig. 6. ANGPTL4 promotes chondrogenesis of mesenchymal cells and HO development via LepR. (A) Representative toluidine blue staining results of hUC-MSCs in indicated conditions (1% Dimethyl sulfoxide (DMSO), ITS, 10 ng/mL leptin, or 10 ng/mL ANGPTL4 treatment for 7 d) to evaluate chondrogenesis differentiation. (B) Representative Micro-CT 3D modeling images of Achilles tendon (sagittal view) of mice in indicated group 8 wk after tenotomy. Red ovals indicate ectopic bones. (C) Quantification of B showing HO volumes of mice in indicated group ($n = 6$ mice per group). Data are represented as mean \pm SEM. ** $P < 0.01$. (D) Representative toluidine blue staining results of primary BMSCs, which were isolated from control (termed NC) or LepR-KO mice, in indicated condition (1% DMSO or 10 ng/mL ANGPTL4) for 7 d. (E) Representative genotyping results of ANGPTL4-KO mice and control littermates (termed NC). Primers used in this experiment are listed in Key Resources Table. (F) Western blotting analysis of ANGPTL4 expression in BAT collected from ANGPTL4-KO (termed KO) or control littermates (Termed NC). α -Tubulin was used as loading control. (G) Representative images for Micro-CT 3D modeling (Left), SOFG staining [Middle; proteoglycan (red), heterotopic bone and Achilles tendon (green)], and Masson staining (Right) of Achilles tendon of mice in indicated strain 8 wk after tenotomy. (H) Quantification of (G, Left) showing HO volumes of mice in indicated strain ($n = 6$ mice per strain). Data are represented as mean \pm SEM. *** $P < 0.001$. See also *SI Appendix*, Fig. S5.

chondrogenesis of mesenchymal cells (42), and the antibody for phospho-NES was not commercially available, the involvement of ANGPTL4-dependent effect on STAT3 pathway was further

investigated. Immunoblotting for total STAT3 and phosphorylated STAT3 confirmed that ANGPTL4 treatment causes global shifts toward STAT3 phosphorylation state in cultured BMSCs

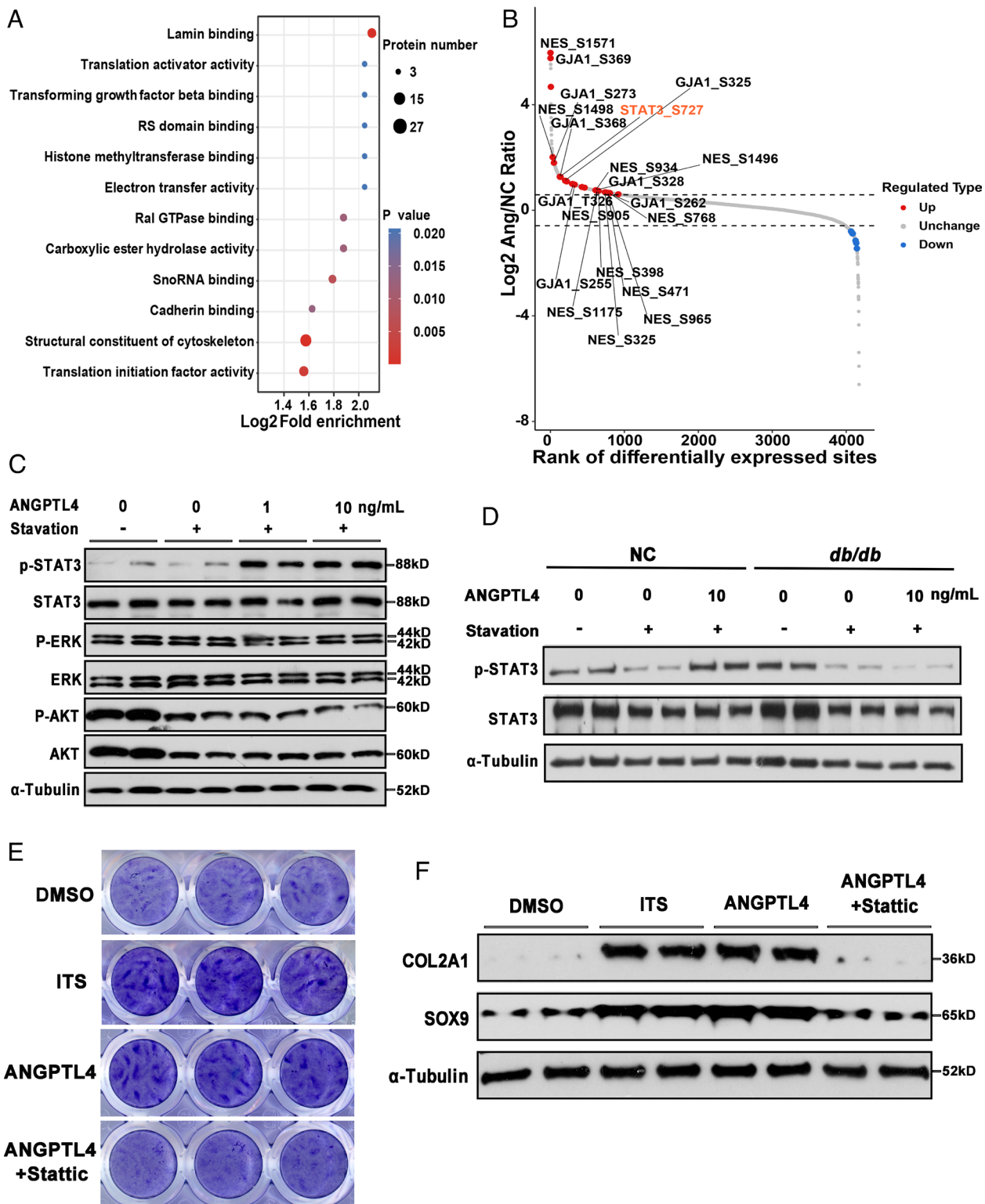


Fig. 7. ANGPTL4-LepR activates STAT3 to promote chondrogenesis in MSCs. (A) Molecular function pathway enrichment analysis of hUC-MSCs treated with ANGPTL4 (10 ng/mL for 30 min) or PBS. (B) Scatter plot and statistics of differentially phosphorylated proteins in hUC-MSCs. (C) Western blotting analysis of STAT3 phosphorylation/total protein, AKT phosphorylation/total protein, and ERK1/2 phosphorylation/total protein in hUC-MSCs stimulated with indicated conditions for 30 min. α -Tubulin was used as loading control. (D) Western blotting analysis of STAT3 phosphorylation/total protein in primary BMSCs isolated from *db/db* or control (termed NC) mice and stimulated with indicated conditions for 30 min. α -Tubulin was used as loading control. (E) Representative toluidine blue staining results of hUC-MSCs in indicated conditions (1% DMSO, ITS, 10 ng/mL ANGPTL4, or 10 ng/mL ANGPTL4 plus 2.5 μ M STAT3 inhibitor Stattic treatment for 7 d) to evaluate chondrogenesis differentiation. (F) Western blotting analysis of COL2A1 and SOX9 in hUC-MSCs stimulated with 1% DMSO, ITS, 10 ng/mL ANGPTL4, or 10 ng/mL ANGPTL4 plus 2.5 μ M STAT3 inhibitor Stattic for 7 d. α -Tubulin was used as loading control.

without alterations in p-ERK/ERK or p-AKT/AKT (Fig. 7C). Accordingly, compared to NC group, MSCs collected from *db/db* mice lost pSTAT3-related response to ANGPTL4 treatment

(Fig. 7D), supporting the LepR-dependent role for ANGPTL4 in activating STAT3 signaling pathway. Meanwhile, this possible mechanism was examined for HO-related function in the context

of chondrogenic differentiation of MSCs. In cultured cells, ANGPTL4 effectively enhanced the toluidine blue staining at 7 d post treatment, whereas Stattic, the selective STAT3 inhibitor, blocked their differentiation toward chondrocytes (Fig. 7 E and F). Taken together, these results support a model wherein ANGPTL4 binds to LepR on mesenchymal cells, activates STAT3 signaling pathway, and in turn promotes their chondrogenic differentiation.

Discussion

Here, we show that ANGPTL4 directly binds to LepR and specifically controls the chondrogenesis process during the development of acquired HO. In this setting, production and secretion of ANGPTL4 in/from BAT binds to LepR on PRRX1⁺ mesenchymal cells and stimulates the LepR-STAT3 signaling axis. Interestingly, our data revealed that ANGPTL4 had higher affinity to LepR than leptin via SPR analysis and functional assessments with respect to chondrogenic differentiation of mesenchymal cells. These results may revise or augment existing paradigms emphasizing the uniqueness of LepR's cognate ligand leptin, and identify ANGPTL4-LepR as a critical regulatory mechanism of chondrogenesis of mesenchymal cells during the development of acquired HO.

Due to the existing paradigms considering leptin as the unique ligand to LepR, most studies investigating functions of LepR-related pathways in controlling physiological homeostasis are relied on simply supplying/removing leptin to/from the system. In this regard, our observation on the difference in the formation of acquired HO between *ob/ob* and *db/db* mice identifies LepR, other than leptin, as the critical regulatory factor, raising the possibility that other ligand(s) may serve as a cue for LepR signaling pathway. The present work indicates that ANGPTL4 binds to LepR on PRRX1⁺ mesenchymal cells during early stage of acquired HO formation and stimulates STAT3 phosphorylation, thus promoting their chondrogenic differentiation. In this setting, ANGPTL4-LepR, other than leptin-LepR, plays roles in the development of acquired HO. ANGPTL4 is a stress and fasting-induced factor and is primarily expressed in the liver, adipose tissue, and ischemic tissues (26, 28, 29). It is well known for its regulatory role in lipid metabolism and glucose homeostasis (43–45). And emerging evidence has revealed its potential therapeutic values in tumorigenesis (46), cardiovascular diseases (47), and diabetic wounds (48). Studies suggest that different ANGPTL4 fragments exhibit plural roles in a tissue-dependent manner. For example, the N-terminal coiled-coil region of ANGPTL4 was shown to be largely responsible for its effect in lipid metabolism and insulin sensitivity (49), and the C-terminal fibrinogen-like domain of ANGPTL4 was identified to be involved in the regulation of vascular junction integrity (50). However, its role in controlling bone formation is unappreciated. Besides, ANGPTL4 has been described to function through different mechanisms, for example, regulating endothelial cell permeability through binding to neuropilin 1 (NRP1) and NRP2 (51), and antagonizing Wnt signaling to promote notochord formation via direct binding to syndecans (52). However, its function through direct binding to LepR has not yet been described. Here, we found that the C-terminal domain of ANGPTL4 interacts with LepR on PRRX1⁺ mesenchymal cells at the HO site and is critical for the chondrogenesis process during ectopic bone formation. Together, our results provide insights into the mechanistic actions of ANGPTL4 and LepR.

During the formation of acquired HO, a series of tightly orchestrated events, namely inflammation, chondrogenesis, and osteogenesis, are observed in the injured tissue or nearby region. Prior work supports a role for the leptin-LepR signaling axis in HO development. For example, clinically, leptin level is higher in female patients whose

ossification of the posterior longitudinal ligament extended to the thoracic and/or lumbar spine (53). And in an animal model, elevated leptin promotes HO formation in rat Achilles tendon after tenotomy (54). Although the specific role of leptin-LepR is not well characterized in terms of acquired HO, wherein other bone formation-related events, a general leverage of leptin-LepR is observed (55). In vitro, leptin is shown to promote the osteogenic differentiation of osteoblasts (56), tendon-derived stem cells, and cells from sites of thoracic ossification of ligament flavum (57). Meanwhile, the chondrogenic differentiation of ATDC5 chondrogenic cells was also shown to be promoted by leptin (58). While leptin-LepR signaling axis seems to have plural roles in controlling bone formation events of multiple cell types, here we specifically show that the ANGPTL4-LepR pathway is critical for mesenchymal cell chondrogenesis during the development of acquired HO, expanding our understanding of LepR in bone formation.

Functional data here identified a critical role for ANGPTL4-LepR in regulating chondrogenesis of mesenchymal cells and eventually the formation of acquired HO, both *in vivo* and *in vitro*. Acquired HO is a frequently observed sequela in patients with trauma and has undergone intensive investigation over the last 50 y due to the increased incidence. Current treatments for HO are restricted to non-steroidal anti-inflammatory drugs (NSAIDs), radiation therapy, and surgical removal (59). NSAIDs could prevent HO by inhibiting the osteogenic differentiation of progenitor cells (60, 61); however, the negative effects of NSAIDs on fracture healing have restricted its clinical application. With respect to radiation therapy and surgical removal, apart from the obvious complications, the recurrence rates (82 to 100% and 17 to 58% respectively) have limited their use. Clearly, the existing therapeutic methods either have poor effect, or exhibit prohibitive risk profiles. In this regard, the crucial role of ANGPTL4 identified here raises the possibility that ANGPTL4-LepR may serve as an efficient target to interrupt chondrogenesis and eventually the formation of acquired HO. Indeed, the present work adds to the known regulatory mechanisms of HO development to propagate a paradigm shift in the approach to manage the pathogenesis of acquired HO.

Materials and Methods

Animals. The animal experiments were conducted in accordance with the guidelines set by the Ethical Committee for Animal Research of Southern Medical University and the Ministry of Science and Technology of China. *db/db*, *ob/ob*, and C57BL/6 mice (4-wk- or 8-wk-old) were purchased from GemPharmatech (Guangzhou, China). The *Prrx1-Cre* (Stock No.: 005584), *LepR^{f/f}* (Stock No.: 008327), *iDTR* (Stock No.: 007900), and *mTmG* (Stock No.: 007676) mouse strains were purchased from Jackson Laboratory. *LepR-Cre* (Stock No.: C001036) mouse strain was purchased from Cyagen Biosciences Inc. *Col2a1-Cre* mouse strain was kind gift from Dr. Xiao Yang. To generate LepR knockout or cell tracing mice, *LepR-Cre* mice were separately crossed with *iDTR* or *mTmG* mice. To generate limb bud mesenchyme/chondrocyte-specific LepR deletion mice, *LepR^{f/f}* mice were crossed with *Prrx1-Cre* or *Col2a1-Cre* mice, respectively. *LepR^{f/f}* mice in the same litter served as control.

The generation of ANGPTL4-KO and ANGPTL4-NKO mice is initiated using CRISPR Design Website (<http://www.e-crisp.org/E-CRISP/>) to design knockout targets for the first exon and the third exon of mouse *Angptl4* gene. The designed targets are as follows: sgRNA target 1-ggtgctatgcggctactgCGG and sgRNA target 2-ggagtagacaagactcgagGGG. SgRNA and Cas9 mRNA were synthesized in vitro and stored at –80 °C for further use. After superovulation and fertilization, 100 ng/μL Cas9 mRNA and 50 ng/μL sgRNA (*Angptl4*-sgRNA1 and *Angptl4*-sgRNA2) were injected into C57BL/6J mouse 1-cell zygote and cultured in K+ Simplex Optimised Medium embryo medium at 37 °C. The cultured embryos were transplanted into the fallopian ampullae of pseudopregnant ICR female mice and then kept for delivery after the wound was sutured. The tail was clipped 21 d after birth to identify the genotypes of mice, and the same mutant mice were routinely bred

in cage until *Angptl4* knockout strain was screened. PCR, western blotting, and IHC were used to verify the knockout effect.

For iDTR treatment experiment, mice were treated with iDTR by intraperitoneal injection at 5 µg/kg/d for up to 7 d at 7 wk and 11 wk after birth. For in vivo experiments with exogenous ANGPTL4, adult C57BL/6J mice were injected with ANGPTL4 protein (5 ng/g of body weight) through the tail vein 3 times per week for 8 wk.

Both male and female mice were utilized and housed in plastic cages under controlled conditions of a temperature of $22 \pm 1^\circ\text{C}$ and a 12-h light/12-h dark cycle. The mice were provided with standard rodent chow and water ad libitum throughout the duration of the study. The primers for genotyping can be found in *SI Appendix, Table S4*.

Cell Culture. Bone marrow MSCs (BMSCs) were isolated from 1-mo-old mice using the EasySep™ Mouse Mesenchymal Stem/Progenitor Cell Enrichment Kit (Stem Cell, Cat#19771). The detailed procedures of BMSCs and additional information regarding cell lines used in this paper can be found in *SI Appendix, Materials and Methods*.

Micro-CT Scanning and Analysis. After the mice were killed, the femur and tibia of the experimental groups were fixed in a 4% paraformaldehyde solution and subsequently subjected to analysis using a Micro-CT scanner with a resolution of 12 µm (Viva CT40; Scanco Medical AG, Bassersdorf, Switzerland). Morphological measurements and 3D reconstruction were conducted utilizing the 2D data obtained from the scan sections. The morphological parameters of the micro-structure, including bone volume/tissue volume, trabecular number, trabecular thickness, and trabecular separation were calculated and defined. Additionally, 3D images were generated using Skyscan Ctvol software (Bruker microCT).

SPR. The mouse LepR, Leptin, and ANGPTL4 protein were purchased from R&D systems. Detailed information is provided in *SI Appendix, Table S4*. After dissolved in running buffer (1 × PBS with 5% DMSO), Leptin or ANGPTL4 protein was fixed on a 3D optical crosslinked chip (Betterways Inc., China) using a Biodot™ AD1520 chip array printer (Biodot Inc., USA). LepR was diluted to a concentration gradient: 200, 400, 800, 1,600, and 3,200 nM flow on the chip surface from low to high concentration. According to the real-time detection results collected from bScreen LB 991 Label-free Microarray System (Berthold Technologies, Germany), the dynamic curve of the interaction is fitted, and the affinity parameters are output.

Molecular Docking Analysis of LepR and ANGPTL4. The 3D structure of protein LepR (P48356-F1-model_v2) and ANGPTL4 (AF-Q9Z1P8-F1-model_v2) were downloaded from AlphaFold Protein Structure Database (<https://alphafold.ebi.ac.uk/>). The binding pattern between LepR and ANGPTL4 was predicted using the protein–protein docking method in ClusPro. Finally, MOE was used for interaction analysis and PyMOL mapping of the selected complex.

Co-IP. ANGPTL4-GST, Leptin-GST, LepR-Flag, LepR-Flag-N, LepR-Flag-C, or pCMV-empty overexpressed plasmids were constructed and co-transfected into HEK293 cells. After transfection, the total protein was lysed 48 h later in a lysis buffer containing 20 mM Tris-HCl, 150 mM NaCl, 0.3% CHAPS, 2 mM EDTA, 0.5 mM dithiothreitol, 1 mM NaF, 1 mM phenylmethylsulfonyl fluoride, and 1× protease inhibitor cocktail (Roche, Basel, Switzerland). Subsequently, centrifugation was performed at 12,000 g for 10 min at 4 °C, and 50 µL of supernatant from each tube was designated as the “input”. The remaining supernatants were incubated overnight at 4 °C with either a Flag-tagged antibody or a control IgG antibody, followed by precipitation using protein G-conjugated sepharose beads (GE Healthcare, Little Chalfont, UK). The agarose beads were then washed six times with 1 mL of lysis buffer before being cracked. To confirm the interaction

between LepR and ANGPTL4, Western blotting analysis was employed to detect the expression of Flag and GST.

Plasmid Construction and Cell Transfection. LepR (Myc-DDK-tagged) 2 (MR226861) was obtained from Origene (Wuxi, China). The LepR sequence-N/C terminals were cloned into pCMV6-Entry Vector between the SfaAI and MluI restriction sites, following the removal of the LepR fragment from LepR (Myc-DDK-tagged) 2. PRK5-GST-Angptl4 and PRK5-GST-Leptin were derived from prk5 HA GST Rheb1 by replacing Rheb1 with the respective Angptl4 or Leptin sequences, utilizing the SalI and NotI restriction sites. pX459-mLepR-sgRNA1, pX459-mLepR-sgRNA2, pX330-mAngptl4-sgRNA-1 and pX330-mAngptl4-sgRNA-2 constructs were generated by sub-cloning the corresponding PCR products, which were annealed from Oligonucleotide primers biosynthesis in the Beijing Tsingke Biotech Co., Ltd. into the BpuI sites of pX459 (mLepR-sgRNA vectors) or pX330 (mAngptl4-sgRNA vectors). The constructs were amplified using the primers listed in the *SI Appendix, Table S4* and verified by sequencing. The plasmids with Flag or GST fusion were transfected into HEK293 as indicated in the figure legends using Lipofectamine 3000 (Cat#L3000-015, Invitrogen, Carlsbad, CA, USA) according to the manufacturer’s recommendations. The plasmids with sgRNA targets were transcript in vitro following instruction for MEGAshortscript™ T7 Kit (Cat#AM1354, Invitrogen, Carlsbad, CA, USA).

Quantification and Statistical Analysis. qRT-PCR data were calculated using the $2^{-\Delta\Delta Ct}$ method. Data were presented as mean values \pm SEM of at least three independent experiments. Independent-sample *t* tests were performed to compare two groups. One-way ANOVA was used for multiple comparisons, the LSD test was used for homogeneity of variance, and Dunnett’s T3 test after Welch’s method was used for inconsistency of variance. The level of significance was set at $P < 0.05$. All data analyses were performed using SPSS 13.0 software (SPSS Inc., Chicago, IL, USA).

Data, Materials, and Software Availability. Phosphoproteomics data (62) have been deposited to the ProteomeXchange Consortium via the PRIDE partner repository with the dataset identifier [PXD043087](https://doi.org/10.3390/pxd043087). Reviewer account details: (Username: reviewer_pxd043087@ebi.ac.uk Password: 1CbQpuBU). Detailed information on the materials and software used in this paper is provided in *SI Appendix*.

ACKNOWLEDGMENTS. This work was supported by grants from the National Natural Science Foundation of China (82301002, 82202654, 92268204, and 81991511), the Guangdong Basic and Applied Basic Research Foundation (2019A1515110148) and the China Postdoctoral Science Foundation (2022M711510 and 2023M731545).

Author affiliations: ^aGuangdong Provincial Key Laboratory of Bone and Joint Degenerative Diseases, The Third Affiliated Hospital of Southern Medical University, Guangzhou, Guangdong 510630, China; ^bDepartment of Trauma and Joint Surgery, Shunde Hospital, Southern Medical University, Foshan, Guangdong 528300, China; ^cDepartment of Biochemistry and Molecular Biology, School of Basic Medical Sciences, Southern Medical University, Guangzhou, Guangdong 510515, China; ^dDepartment of Orthopaedics, The Fifth Affiliated Hospital, Southern Medical University, Guangzhou, Guangdong 510900, China; ^eDepartment of Cell Biology, School of Basic Medical Sciences, Southern Medical University, Guangzhou, Guangdong 510515, China; ^fDepartment of Orthopaedics, Nanfang Hospital, Southern Medical University, Guangzhou, Guangdong 510515, China; ^gDepartment of Developmental Biology, School of Basic Medical Sciences, Southern Medical University, Guangzhou, Guangdong 510515, China; ^hDepartment of Pathology, Nanfang Hospital, School of Basic Medical Sciences, Southern Medical University, Guangzhou, Guangdong 510515, China; ⁱDepartment of Pharmacology and Chemical Biology, University of Pittsburgh School of Medicine, Pittsburgh, PA 15261; and ^jDepartment of Orthopaedics, The Tenth Affiliated Hospital, Southern Medical University, Dongguan, Guangdong 523018, China

1. Y. Zhang *et al.*, Positional cloning of the mouse obese gene and its human homologue. *Nature* **372**, 425–432 (1994).
2. J. M. Friedman, J. L. Halaas, Leptin and the regulation of body weight in mammals. *Nature* **395**, 763–770 (1998).
3. G. H. Lee *et al.*, Abnormal splicing of the leptin receptor in diabetic mice. *Nature* **379**, 632–635 (1996).
4. R. J. Perry *et al.*, Leptin mediates a glucose-fatty acid cycle to maintain glucose homeostasis in starvation. *Cell* **172**, 234–248.e17 (2018).
5. A. W. Fischer, B. Cannon, J. Nedergaard, Leptin: Is it thermogenic? *Endocrine Rev.* **41**, 232–260 (2020).
6. C. Berger, N. Klöting, Leptin receptor compound heterozygosity in humans and animal models. *Int. J. Mol. Sci.* **22**, 4475 (2021).
7. F. Suriano *et al.*, Novel insights into the genetically obese (ob/ob) and diabetic (db/db) mice: Two sides of the same coin. *Microbiome* **9**, 147 (2021).
8. P. Ducey *et al.*, Leptin inhibits bone formation through a hypothalamic relay: A central control of bone mass. *Cell* **100**, 197–207 (2000).
9. G. Karsenty, Convergence between bone and energy homeostases: Leptin regulation of bone mass. *Cell Metab.* **4**, 341–348 (2006).
10. G. Karsenty, S. Khosla, The crosstalk between bone remodeling and energy metabolism: A translational perspective. *Cell Metab.* **34**, 805–817 (2022).
11. B. O. Zhou, R. Yue, M. M. Murphy, J. G. Peyer, S. J. Morrison, Leptin-receptor-expressing mesenchymal stromal cells represent the main source of bone formed by adult bone marrow. *Cell Stem Cell* **15**, 154–168 (2014).

12. B. Shen *et al.*, A mechanosensitive peri-arteriolar niche for osteogenesis and lymphopoiesis. *Nature* **591**, 438–444 (2021).
13. T. Thomas *et al.*, Leptin acts on human marrow stromal cells to enhance differentiation to osteoblasts and to inhibit differentiation to adipocytes. *Endocrinology* **140**, 1630–1638 (1999).
14. E. L. Scheller *et al.*, Leptin functions peripherally to regulate differentiation of mesenchymal progenitor cells. *Stem Cells* **28**, 1071–1080 (2010).
15. R. Yue, B. O. Zhou, I. S. Shimada, Z. Zhao, S. J. Morrison, Leptin receptor promotes adipogenesis and reduces osteogenesis by regulating mesenchymal stromal cells in adult bone marrow. *Cell Stem Cell* **18**, 782–796 (2016).
16. R. T. Turner *et al.*, Peripheral leptin regulates bone formation. *J. Bone Miner. Res.* **28**, 22–34 (2013).
17. C. Meyers *et al.*, Heterotopic ossification: A comprehensive review. *JBMR plus* **3**, e10172 (2019).
18. Y. Xu *et al.*, Heterotopic ossification: Clinical features, basic researches, and mechanical stimulations. *Front. Cell Dev. Biol.* **10**, 770931 (2022).
19. Q. Zhang, D. Zhou, H. Wang, J. Tan, Heterotopic ossification of tendon and ligament. *J. Cell. Mol. Med.* **24**, 5428–5437 (2020).
20. D. Dey *et al.*, Two tissue-resident progenitor lineages drive distinct phenotypes of heterotopic ossification. *Sci. Transl. Med.* **8**, 366ra163 (2016).
21. L. Vanden Bossche, G. Vanderstraeten, Heterotopic ossification: A review. *J. Rehabil. Med.* **37**, 129–136 (2005).
22. S. Agarwal *et al.*, Inhibition of Hif1 α prevents both trauma-induced and genetic heterotopic ossification. *Proc. Natl. Acad. Sci. U.S.A.* **113**, E338–E347 (2016).
23. S. Agarwal *et al.*, Scleraxis-lineage cells contribute to ectopic bone formation in muscle and tendon. *Stem Cells* **35**, 705–710 (2017).
24. S. Agarwal *et al.*, BMP signaling mediated by constitutively active Activin type 1 receptor (ACVR1) results in ectopic bone formation localized to distal extremity joints. *Dev. Biol.* **400**, 202–209 (2015).
25. J. B. Regard *et al.*, Activation of Hedgehog signaling by loss of GNAS causes heterotopic ossification. *Nat. Med.* **19**, 1505–1512 (2013).
26. S. Kersten *et al.*, Characterization of the fasting-induced adipose factor FIAF, a novel peroxisome proliferator-activated receptor target gene. *J. Biol. Chem.* **275**, 28488–28493 (2000).
27. P. M. M. Ruppert *et al.*, Fasting induces ANGPTL4 and reduces LPL activity in human adipose tissue. *Mol. Metab.* **40**, 101033 (2020).
28. I. Kim *et al.*, Hepatic expression, synthesis and secretion of a novel fibrinogenangiopoietin related protein that prevents endothelial-cell apoptosis. *Biochem. J.* **346**, 603–610 (2000).
29. J. C. Yoon *et al.*, Peroxisome proliferator-activated receptor gamma target gene encoding a novel angiopoietin-related protein associated with adipose differentiation. *Mol. Cell. Biol.* **20**, 5343–5349 (2000).
30. C. Fernandez-Hernando, Y. Suarez, ANGPTL4: A multifunctional protein involved in metabolism and vascular homeostasis. *Curr. Opin. Hematol.* **27**, 206–213 (2020).
31. M. Ploug, ANGPTL4: A new mode in the regulation of intravascular lipolysis. *Curr. Opin. Lipidol.* **33**, 112–119 (2022).
32. A. S. Tiffany, B. A. C. Harley, Growing pains: The need for engineered platforms to study growth plate biology. *Adv. Healthcare Mater.* **11**, e2200471 (2022).
33. R. Foisner, L. Gerace, Integral membrane proteins of the nuclear envelope interact with lamins and chromosomes, and binding is modulated by mitotic phosphorylation. *Cell* **73**, 1267–1279 (1993).
34. K. Furukawa, T. Kondo, Identification of the lamina-associated-polypeptide-2-binding domain of B-type lamin. *Eur. J. Biochem.* **251**, 729–733 (1998).
35. I. Duband-Goulet, J. C. Courvalin, B. Buendia, LBR, a chromatin and lamin binding protein from the inner nuclear membrane, is proteolyzed at late stages of apoptosis. *J. Cell Sci.* **111**, 1441–1451 (1998).
36. J. C. Choi, H. J. Worman, Nuclear envelope regulation of signaling cascades. *Adv. Exp. Med. Biol.* **773**, 187–206 (2014).
37. D. Camozzi *et al.*, Diverse lamin-dependent mechanisms interact to control chromatin dynamics. Focus on laminopathies. *Nucleus* **5**, 427–440 (2014).
38. J. Mateos *et al.*, Lamin A deregulation in human mesenchymal stem cells promotes an impairment in their chondrogenic potential and imbalance in their response to oxidative stress. *Stem Cell Res.* **11**, 1137–1148 (2013).
39. M. Attur *et al.*, Perturbation of nuclear lamin A causes cell death in chondrocytes. *Arthritis Rheum.* **64**, 1940–1949 (2012).
40. D. L. Hevehan, W. M. Miller, E. T. Papoutsakis, Differential expression and phosphorylation of distinct STAT3 proteins during granulocytic differentiation. *Blood* **99**, 1627–1637 (2002).
41. T. Xia *et al.*, Advances in the role of STAT3 in macrophage polarization. *Front. Immunol.* **14**, 1160719 (2023).
42. M. Kondo *et al.*, Contribution of the interleukin-6/STAT-3 signaling pathway to chondrogenic differentiation of human mesenchymal stem cells. *Arthritis Rheumatol.* **67**, 1250–1260 (2015).
43. V. Sukonina, A. Lookene, T. Olivecrona, G. Olivecrona, Angiopoietin-like protein 4 converts lipoprotein lipase to inactive monomers and modulates lipase activity in adipose tissue. *Proc. Natl. Acad. Sci. U.S.A.* **103**, 17450–17455 (2006).
44. Y. Oike, M. Akao, Y. Kubota, T. Suda, Angiopoietin-like proteins: Potential new targets for metabolic syndrome therapy. *Trends Mol. Med.* **11**, 473–479 (2005).
45. A. Xu *et al.*, Angiopoietin-like protein 4 decreases blood glucose and improves glucose tolerance but induces hyperlipidemia and hepatic steatosis in mice. *Proc. Natl. Acad. Sci. U.S.A.* **102**, 6086–6091 (2005).
46. M. J. Tan, Z. Teo, M. K. Sng, P. Zhu, N. S. Tan, Emerging roles of angiopoietin-like 4 in human cancer. *Mol. Cancer Res.* **10**, 677–688 (2012).
47. S. Shuff, Y. Oyama, L. Walker, T. Eickle, Circadian angiopoietin-like-4 as a novel therapy in cardiovascular disease. *Trends Mol. Med.* **27**, 627–629 (2021).
48. Y. Y. Goh *et al.*, Angiopoietin-like 4 interacts with matrix proteins to modulate wound healing. *J. Biol. Chem.* **285**, 32999–33009 (2010).
49. H. Ge, G. Yang, X. Yu, T. Pourbahrami, C. Li, Oligomerization state-dependent hyperlipidemic effect of angiopoietin-like protein 4. *J. Lipid Res.* **45**, 2071–2079 (2004).
50. R. L. Huang *et al.*, ANGPTL4 modulates vascular junction integrity by integrin signaling and disruption of intercellular VE-cadherin and claudin-5 clusters. *Blood* **118**, 3990–4002 (2011).
51. A. Sodhi *et al.*, Angiopoietin-like 4 binds neuropilins and cooperates with VEGF to induce diabetic macular edema. *J. Clin. Invest.* **129**, 4593–4608 (2019).
52. N. Kirsch *et al.*, Angiopoietin-like 4 is a wnt signaling antagonist that promotes LRP6 turnover. *Dev. Cell* **43**, 71–82.e6 (2017).
53. Y. Ikeda *et al.*, Association between serum leptin and bone metabolic markers, and the development of heterotopic ossification of the spinal ligament in female patients with ossification of the posterior longitudinal ligament. *Eur. Spine J.* **20**, 1450–1458 (2011).
54. H. Jiang *et al.*, Leptin accelerates the pathogenesis of heterotopic ossification in rat tendon tissues via mTORC1 signaling. *J. Cell Physiol.* **233**, 1017–1028 (2018).
55. I. R. Reid, P. A. Baldock, J. Cornish, Effects of leptin on the skeleton. *Endocrine Rev.* **39**, 938–959 (2018).
56. A. E. Handschin *et al.*, Leptin increases extracellular matrix mineralization of human osteoblasts from heterotopic ossification and normal bone. *Ann. Plast. Surg.* **59**, 329–333 (2007).
57. D. Fan, Z. Chen, Y. Chen, Y. Shang, Mechanistic roles of leptin in osteogenic stimulation in thoracic ligament flavum cells. *J. Biol. Chem.* **282**, 29958–29966 (2007).
58. M. Ben-Elizer, M. Phillip, G. Gat-Yablonski, Leptin regulates chondrogenic differentiation in ATDC5 cell-line through JAK/STAT and MAPK pathways. *Endocrine* **32**, 235–244 (2007).
59. C. D. Hwang *et al.*, Contemporary perspectives on heterotopic ossification. *JCI insight* **7**, e158996 (2022).
60. J. K. Chang *et al.*, Effects of anti-inflammatory drugs on proliferation, cytotoxicity and osteogenesis in bone marrow mesenchymal stem cells. *Biochem. Pharmacol.* **74**, 1371–1382 (2007).
61. J. K. Chang *et al.*, Anti-inflammatory drugs suppress proliferation and induce apoptosis through altering expressions of cell cycle regulators and pro-apoptotic factors in cultured human osteoblasts. *Toxicology* **258**, 148–156 (2009).
62. H. Hu, Phosphoproteomics data. PRIDE Archive. <https://www.ebi.ac.uk/pride/archive/projects/PXD043087/private>. Accessed 19 June 2023.